ORIGINAL RESEARCH

Fabrication of Interleukin-4 Encapsulated Bioactive Microdroplets for Regulating Inflammation and Promoting Osteogenesis

Yi Zhang[1,*], Jin Cao[2,*], Minghui Jian[1], Zhixiao Zhou[2], Nadia Anwar[2], Lan Xiao [3,4], Yaping Ma[2], Dingmei Zhang[2], Jun Zhang[2], Xin Wang[1–4]

[1]Department of Hygiene Toxicology, Zunyi Medical University, Zunyi, Guizhou, 563000, People's Republic of China; [2]Department of Orthopaedic Surgery, Affiliated Hospital of Zunyi Medical University, Zunyi, Guizhou, 563003, People's Republic of China; [3]School of Mechanical, Medical and Process Engineering, Centre for Biomedical Technologies, Queensland University of Technology, Brisbane, QLD, 4059, Australia; [4]Australia-China Centre for Tissue Engineering and Regenerative Medicine, Queensland University of Technology, Brisbane, QLD, 4059, Australia

*These authors contributed equally to this work

Correspondence: Xin Wang, Department of Orthopaedic Surgery, Affiliated Hospital of Zunyi Medical University, Zunyi, Guizhou, 563003, People's Republic of China, Tel +86 136 3928 8558, Fax +86-851-2860 8903, Email lchwx@aliyun.com

Background: Despite the inherent regenerative ability of bone, large bone defect regeneration remains a major clinical challenge for orthopedic surgery. Therapeutic strategies medicated by M2 phenotypic macrophages or M2 macrophage inducer have been widely used to promote tissue remodeling. In this study, ultrasound-responsive bioactive microdroplets (MDs) encapsulated with bioactive molecule interleukin-4 (IL4, hereafter designated MDs-IL4) were fabricated to regulate macrophage polarization and potentiate the osteogenic differentiation of human mesenchymal stem cells (hBMSCs).

Materials and Methods: The MTT assay, live and dead staining, and phalloidin/DAPI dual staining were used to evaluate biocompatibility in vitro. H&E staining was used to evaluate biocompatibility in vivo. Inflammatory macrophages were further induced via lipopolysaccharide (LPS) stimulation to mimic the pro-inflammatory condition. The immunoregulatory role of the MDs-IL4 was tested via macrophage phenotypic marker gene expression, pro-inflammatory cytokine level, cell morphological analysis, and immunofluorescence staining, etc. The immune-osteogenic response of hBMSCs via macrophages and hBMSCs interactions was further investigated in vitro.

Results: The bioactive MDs-IL4 scaffold showed good cytocompatibility in RAW 264.7 macrophages and hBMSCs. The results confirmed that the bioactive MDs-IL4 scaffold could reduce inflammatory phenotypic macrophages, as evidenced by changing in morphological features, reduction in pro-inflammatory marker gene expression, increase of M2 phenotypic marker genes, and inhibition of pro-inflammatory cytokine secretion. Additionally, our results indicate that the bioactive MDs-IL4 could significantly enhance the osteogenic differentiation of hBMSCs via its potential immunomodulatory properties.

Conclusion: Our results demonstrate that the bioactive MDs-IL4 scaffold could be used as novel carrier system for other pro-osteogenic molecules, thus having potential applications in bone tissue regeneration.

Keywords: IL-4, bioactive microdroplets, biocompatibility, macrophages, immunoregulation, osteogenesis

Introduction

Bone fracture or bone defects are a serious public health issue globally, especially in aged population or people with osteoporosis.[1] It is estimated that more than 8.9 million fractures were recorded annually, posing huge economic burden on society and family.[2] Treatment of bone fracture includes internal stabilization with insertion of metal rods or plates, which could restore the damaged bone to its pre-fracture composition.[3] It is estimated that 5% to 10% of fracture cases will develop in the form of delayed union or nonunion fractures, which will have significant impact on patients' life quality.[4] Autograft from iliac crest remains the gold standard for speeding up the bone healing in delayed fractures.[5] However, the limited supply from the

donor site makes this an unideal method. In addition, many synthetic bone grafts and tissue engineered micro- or nano-scaffolds were fabricated to enhance the osteogenic differentiation of stem cells and bone regeneration.[6]

As one of the most important cells in innate and adaptative immunity, macrophages play a vital role in regulating the immune response, inflammation, and subsequent tissue repair.[7] Macrophages are highly versatile cells that can adapt to the microenvironment by polarizing into pro-inflammatory phenotype M1 phenotype or alternately activated anti-inflammatory phenotype M2 macrophages.[8] Uncontrolled M1 polarized macrophages increase bone resorption through various mechanisms, including secretion of large amount of pro-inflammatory cytokines (including but not limited to high levels of IL-12 (Interleukin 12), IL-6, TNF-α (Tumor Necrosis Factor α), IL-1α, IL-1β), chemokines (CCL-2 and IL-8), metalloproteinases (MMP-3 and MMP-12), and increases osteoclast differentiation potential.[9] Prolonged inflammatory macrophage activation results in significant tissue damage and a chronic inflammatory state, leading to chronic inflammatory autoimmune diseases such as osteoporosis and rheumatoid arthritis (RA). Therefore, therapeutic interventions that targeting activated M1 macrophages have been frequently applied to accelerate wound healing and tissue regeneration.[10] For example, granulocyte-macrophage colony stimulating factor (GM-CSF) is one possible inducer of M1 polarization.[11] Blocking GM-CSF has been shown therapeutic efficacy in RA mouse models and has also been used in several clinical trials in RA patients.[12] Interleukin-4 (IL-4) is a classical inducer for M2 macrophages. IL-4 has been widely used as encapsulating molecules in various biomaterials scaffolds as potential therapeutic strategies for tissue regeneration. For example, Gong et al developed IL-4-loaded bi-layer scaffold that could promote the cartilage and subchondral bone regeneration.[13] Ueno et al also generated IL-4 overexpressing MSCs modified macroporous scaffold and found enhanced bone regeneration in critical-size bone defect model.[14] Therefore, developing novel biomaterials with immunoregulatory properties holds significant clinical translation promise.

Ultrasound, including low frequency (<100kHz) and high frequency (>100kHz and MHz range), has been shown to enhance drugs/gene delivery efficiency.[15] Microbubbles (MBs) or nanobubbles (NBs), as ultrasonic response materials, can enhance permeability and drug accumulation and retention in tissues due to their excellent therapeutic size.[16] For example, previous study using doxorubicin-loaded microbubbles and ultrasound-guided delivery system and found markedly inhibitory effect on the melanoma cells.[17] Even in articular cartilage, which is difficult to transport, ultrasonic-responsive microbubbles can greatly improve transport efficiency. Additionally, modification of the bubbles with specific cargos, including targeted delivery of genes, siRNA and cytokines, have also demonstrated remarkable therapeutic effects.[18] Therefore, micro- or nanobubbles-based therapy represents a promising therapeutic approach for drugs/gene delivery system to enhance delivery efficiency and improve tissue repair.

Therefore, in this study, we intend to generate a novel IL4-based microdroplets delivery strategy to regulate inflammation, which in turn, influences the process of osteogenic differentiation. This study provides a novel therapeutic option in the prevention and treatment of inflammation-mediated delayed bone healing or other inflammatory bone diseases.

Materials and Methods
Cell Culture

Human bone marrow-derived mesenchymal stromal cells (hBMSCs, ATCC® PCS-500-012™) were used for osteogenic differentiation in this study. Briefly, cells were cultured in Dulbecco's Modified Eagle's Medium (DMEM; Life Technologies Pty Ltd., China) containing 10% fetal bovine serum (FBS; Biological Industries, LTD, Beit Haemek, Israel), and 1% penicillin/streptomycin (Solarbio, Beijing, China) in a 5% CO2 humidified incubator at 37°C. The murine-derived macrophage cell line RAW264.7 cells (ATCC® TIB-71™) were maintained in DMEM containing 10% heat-inactivated FBS, 1% penicillin/streptomycin in a humidified incubator containing 5% CO_2 at 37°C.

Fabrication and Characterization of Bioactive MDs-IL4

The bovine serum albumin (BSA)-stabilized IL-4 MDs was fabricated according to previous studies.[18,19] 100 ng/mL IL-4 (R&D system, China) was used based on a previous study.[20] Briefly, 100 ng/mL IL-4, 300 μL perfluorocarbon, and 4 mL of PBS, and 40 mg of bovine serum albumin (BSA, Sigma Aldrich, China) were used for MDs fabrication. The resulting

emulsion was ultracentrifuged (Beckman Coulter, Optima XPN-100, USA) at 14,000 rpm for 30 min, and the MDs-IL4 were used for subsequent testing. To generate fluorescence-labeled MDs for fluorescence imaging, fluorescein isothiocyanate (FITC)-labelled BSA (Sigma Aldrich, China) was used for MDs fabrication. Fluorescence-labeled MDs-IL4 were used for MDs characterization using a confocal laser scanning microscopy (CLSM). Briefly, 50 mg MDs-IL4 were diluted into PBS and then observed using a confocal laser scanning microscope with a ×40 objective (Leica DM IRB; Leica, Wetzlar, Germany). MDs-IL4 growth and rupture were observed using an inverted light microscope (Leica, Wetzlar, Germany). Briefly, the samples were exposed to an ultrasound probe with an acoustic frequency 1 MHz by portable home use ultrasound pain therapy device for 25 min (MYCHWAY, China). Images were captured using an inverted light microscope (Leica, Wetzlar, Germany).

MTT Assay

In vitro biocompatibility of MDs was determined using MTT cell proliferation assay according to the manufacturer's instructions. Briefly, cells were placed in 96-wells plate overnight and then treated with different formulation of MDs. At the end of the incubation, 20 μL of 5 mg/mL 3-(4, 5-dimethylthiazol-2-yl)-2, 5-diphenyl tetrazolium bromide (MTT, M2128, Sigma, China) was added to each well. After incubation for 2–4 h, the purple formazan formed was dissolved using 100 μL dimethyl sulfoxide (DMSO). The absorbance was read at 570 nm using a microplate spectrophotometer.

Live and Dead Cell Assay

Live and dead cell assay was performed using the Live and Dead Cell Assay kit following the manufacturer's instructions (ab115347, Abcam, China). Briefly, cells were treated with different formulation of MDs. At the end of the treatment, cells were stained with the Live and Dead Dye diluted in PBS for 10 min at room temperature in the dark. Images were captured using a confocal laser scanning microscope with a ×10 objective (Leica DM IRB; Leica, Wetzlar, Germany).

Cell Morphological Analysis

Cell morphology was examined by confocal laser scanning microscopy via phalloidin/DAPI staining. Briefly, the samples were treated with different formulation of MDs, rinsed with PBS, fixed at room temperature with 4% paraformaldehyde, permeabilized, and stained with Alexa Fluor 594-labeled phalloidin (Thermo Fisher Scientific, China) for 1 h. Samples were then mounted with ProLong™ Gold Antifade Mountant with DAPI (P36935, Thermo Fisher Scientific, China) and the images of the stained samples were examined using a confocal laser scanning microscope with a ×10 objective (Leica DM IRB; Leica, Wetzlar, Germany).

Macrophage Polarization and Cell Morphological Analysis

Macrophages were activated with LPS according to a previous study.[21] Briefly, macrophages were seeded on 24-well tissue culture coverslip overnight, then stimulated with 1000 ng/mL of Lipopolysaccharide (LPS, Escherichia coli 0111: B4, Sigma, China) for 12 h. Cells were rinsed with PBS three times, then treated with different formulation of MDs for 12 h. Conditioned medium (CM) from RAW264.7 cells stimulated with or without different formulation of MDs were collected for subsequent analysis. CM were centrifuged at 2000 g for 10 min 4°C, then filtered using a 0.2 μm filter to remove cell debris. CM was aliquoted (designated as control-CM, MDs-CM, MDs-IL4-CM) and stored at −80°C before usage. Cell morphological analysis was performed using Alexa Fluor 594-labeled phalloidin/DAPI double staining and was examined by confocal laser scanning microscopy. Briefly, cells were subjected to 4% paraformaldehyde fixation for 10 min followed by permeabilization using 0.25% Triton X-100. Alexa Fluor 594-labeled phalloidin (Thermos Fisher Scientific, China) and DAPI staining were performed following the manufacturer's protocol to visualize actin filaments and the nucleus, respectively. Samples were mounted with ProLong™ Gold Antifade Mountant (Thermo Fisher Scientific, China) and the images captured using a confocal laser scanning microscope with a ×40 objective (Leica DM IRB; Leica, Wetzlar, Germany).

Enzyme-Linked Immunosorbent Assay (ELISA)

The expression of pro-inflammatory cytokine interleukin 6 (IL-6) was evaluated by ELISA according to the manufacturer's instructions (M6000B, R&D systems, China). Briefly, 50 μL of Assay Diluent was added into each well of the ELISA plate before adding 50 μL of the standard or the samples. The plate was covered with a plate sealer and incubated at room temperature for 2 hours. The ELISA plate was thoroughly washed with washing buffer with a total of 5 washes before adding 100 μL of Conjugate to each well. The plate was covered with a plate sealer and incubated at room temperature for 2 hours. Aspiration and washing step were repeated 5 times again. Next, 100 μL Substrate Solution was added into each well and incubated at room temperature for 30 minutes, prior to the addition of 100 μL Stop Solution. The absorbance was read at 450 nm using a microplate spectrophotometer with a reference absorbance at 570 nm. The concentrations of pro-inflammatory cytokine were quantified based on the standard curve.

Immunofluorescent Staining

Immunofluorescent staining was used to assess the iNOS expression. Briefly, cells were washed with PBS twice and fixed with 4% paraformaldehyde for 10 min at room temperature. Cells were permeabilized with 0.25% Triton X-100 for 10 min and blocked with 4% bovine serum albumin (BSA) for 1 h at room temperature. After rinsing with PBS twice, cells were incubated with rabbit polyclonal to iNOS (ab178945, Abcam) overnight at 4°C. The next day, cells were rinsed in PBS and incubated with Fluorescein isothiocyanate-conjugated goat anti-rabbit IgG (H+L) secondary antibody for 1 h. After three times rinsing in PBS, cells were counterstained with Alexa Fluor 594-labeled phalloidin followed by DAPI staining as described above. Images were acquired using a confocal laser scanning microscope with a ×20 objective (Leica DM IRB; Leica, Wetzlar, Germany).

Quantitative Real-Time RT-PCR (qPCR)

Total RNA was isolated using TRIzol® reagent (15596018, Thermo Fisher Scientific, China) according to manufacturer's instruction. RNA concentration and purity were determined using a NanoDrop 8000 spectrophotometer (NanoDrop technologies). 500 ng of total RNA sample was reverse transcribed using a RevertAid First Strand cDNA Synthesis Kit (K1622, Thermo Fisher Scientific, China) and stored at −80°C. Quantitative real-time PCR was performed using SYBR Green qPCR Master Mix (Life Technologies, China) on an ABI Prism 7500 Thermal Cycler (Applied Biosystems, Foster City, California, USA). The target gene expression was normalized to the housekeeping gene glyceraldehyde-3-phosphate dehydrogenase (GAPDH). The difference between the mean Ct values of the gene of interest and the housekeeping gene was labelled ΔCt and the relative expression was calculated using the comparative Ct ($2^{-\Delta\Delta CT}$) method.

hBMSCs Osteogenic Differentiation

For osteogenic differentiation, hBMSCs were cultured with 1:1 ratio of CM and osteogenic differentiation medium (DMEM supplemented with 10% FBS, 1% P/S and 10 mM β-glycerophosphate, 50 mM L-ascorbic acid 2-phosphate, 100 nM dexamethasone). Immunofluorescent staining for early osteogenic differentiation marker (ALP) was performed at 14 days. Briefly, the cells were fixed in 4% paraformaldehyde, permeabilized with 0.25% Triton X-100, then blocked with 4% BSA before incubating with rabbit polyclonal to ALP (ab224335, Abcam) overnight at 4°C. After washing, the cells were incubated with Fluorescein isothiocyanate-conjugated goat anti-rabbit IgG (H+L) secondary antibody for 1 h. Actin filaments and cell nuclei were counterstained with Alexa Fluor 594-labeled phalloidin and DAPI as described above. Images were acquired using a confocal laser scanning microscope (Leica DM IRB; Leica, Wetzlar, Germany). The expression of osteogenic-related marker genes was evaluated by qPCR as described above.

ALP Staining

ALP staining was performed to assess osteoblastic differentiation in hBMSCs at 14 days. ALP staining was performed using BCIP/NBT Alkaline phosphatase Color Development Kit according to the manufacturer's instruction (Beyotime, Shanghai, China). Images were acquired using inverted light microscope (Leica, Wetzlar, Germany).

Alizarin Red S Staining

Alizarin red S staining was performed to assess mineral deposits in hBMSCs at 21 days. Briefly, hBMSCs were washed with PBS twice, fixed by 4% paraformaldehyde for 20 min at room temperature. After rinsing in water, samples were then stained with 2% Alizarin Red S staining solution (pH = 4.1) for 20 min at room temperature. Images were taken using inverted light microscope (Leica, Wetzlar, Germany). 10% (v/w) cetylpyridinium chloride (CPC; Sigma, China) in sodium phosphate was used to quantify Alizarin red S staining.

Animal Study

All animal experiments were in accord with institutional animal use and care regulations approved by the Zunyi Medical University Committee (ZMU21-2203-009). Albumin from rat serum was purchased from Sigma Aldrich, China. Male rats (Sprague Dawley, 8 weeks old) were used for the in vivo study. The animals were housed in a standard laboratory environment. The rats were divided into two groups for intraperitoneal (*I.P.*) injection: saline injection (n = 4), saline+MDs-IL-4 (20 mg/kg) injection (n = 4).

Histological Analysis

The major organs including spleen, kidney, and lung were harvested from the sacrificed animals at days 7 and then fixed in 10% neutral buffered formalin for 48 hours. Tissues were embedded in paraffin, sectioned (5 μm), and stained using standard hematoxylin-eosin (H&E) method. Images of the stained sections were examined using an inverted microscope (Leica, Wetzlar, Germany).

Statistical Analysis

All data were expressed as mean ± standard deviations (SD). Statistical analysis was performed using GraphPad Prism 7 (Version 7.02) for Windows (GraphPad Software Inc., USA). Statistical differences between groups were determined with one-way analysis of variance (ANOVA) with Bonferroni's multiple comparison-tests. A value of $p < 0.05$ was considered statistically significant.

Results
Synthesis and Characterization of Bioactive MDs-IL4

The purpose of this work was to fabricate ultrasound-sensitive bioactive microdroplets that can regulate inflammation and osteogenesis. Therefore, we first fabricated microdroplets architecture with the encapsulation of bioactive molecule IL-4 (MDs-IL4). As shown in Figure 1A, confocal laser scanning microscopy images demonstrated spherical morphology microdroplets with a well-defined core-shell structure.

MDs-IL4 response to ultrasound was further examined via phase contrast imaging. As shown in Figure 1B, we observed gradual expansion of MDs-IL4 gas core from 30 min to 90 min, indicating good response of MDs-IL4 to ultrasound stimulation.

Biocompatibility of Bioactive MDs in Macrophages

To investigate whether bioactive MDs affect macrophage viability, MTT cell proliferation assay was first performed. As shown in Figure 2A and B, MTT assay demonstrated that MDs alone or MDs-IL4 did not inhibit the proliferation of RAW264.7 cells when compared with the non-treated control cells. Additionally, the viability between MDs- and MDs-IL4 group showed no difference, suggesting that our bioactive MDs showed good biocompatibility in macrophages. We next investigated the biocompatibility of our bioactive MDs in macrophages using live/dead staining. As shown in Figure 2C and D, the live/dead staining results revealed that macrophages showed green fluorescence staining in all three testing groups. These results indicate that both MDs and MDs-IL4 exhibited a good level of cytocompatibility compared to the non-treated control.

We next evaluated the effects of different formulation of MDs on RAW 264.7 macrophages via phalloidin and DAPI staining. As shown in Figure 2E and F, phalloidin and DAPI staining demonstrated similar growth patterns among different groups, indicating no significant toxic effects.
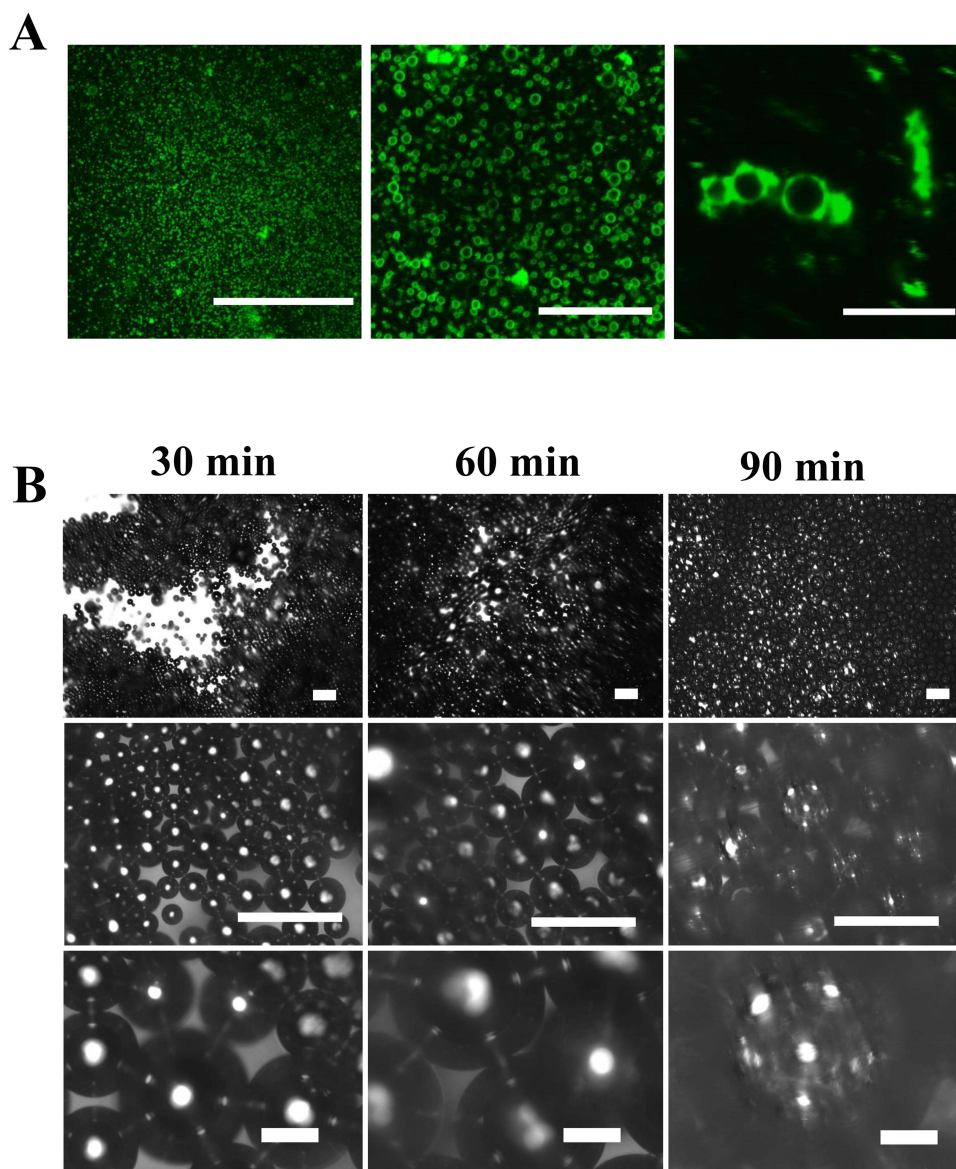
Figure I Fabrication of bioactive MDs-IL4. (**A**) Representative CLSM images of fluorescence labeled bioactive MDs-IL4. Scale bar = 200 μm (left), scale bar = 20 μm (middle), Scale bar = 10 μm (right). (**B**) Representative MDs-IL4 growth and rupture micrographs. Ultrasound leads to the expansion and rupture of MD-IL4. Scale bar = 500 μm (top panel), scale bar = 500 μm (middle panel), Scale bar = 100 μm (bottom panel).

Biocompatibility of Bioactive MDs in hBMSCs

To investigate the biocompatibility of our bioactive MDs on the hBMSCs, MTT cell proliferation assay was performed. In the MTT assay for the cytocompatibility analysis using hBMSCs, the viability in both the MDs group and MDs-IL4 group showed no difference when compared to the values in the control group (Figure 3A and B). The hBMSCs treated with the bioactive MDs were further subjected to double live and dead staining to obtain evidence for viability changes. Both MDs and MDs-IL4 groups exhibited extensively green color with no significant morphological changes among different groups (Figure 3C and D). This result further indicates that both MDs and MDs-IL4 treatment showed good cytocompatibility in hBMSCs.

We next evaluated the effects of different formulation of MDs on hBMSCs via phalloidin and DAPI staining. As shown in Figure 3E and F, phalloidin and DAPI staining demonstrated similar growth patterns among different groups. Additionally, MSCs showed intense cytoskeleton staining with no significant morphological changes among different groups.
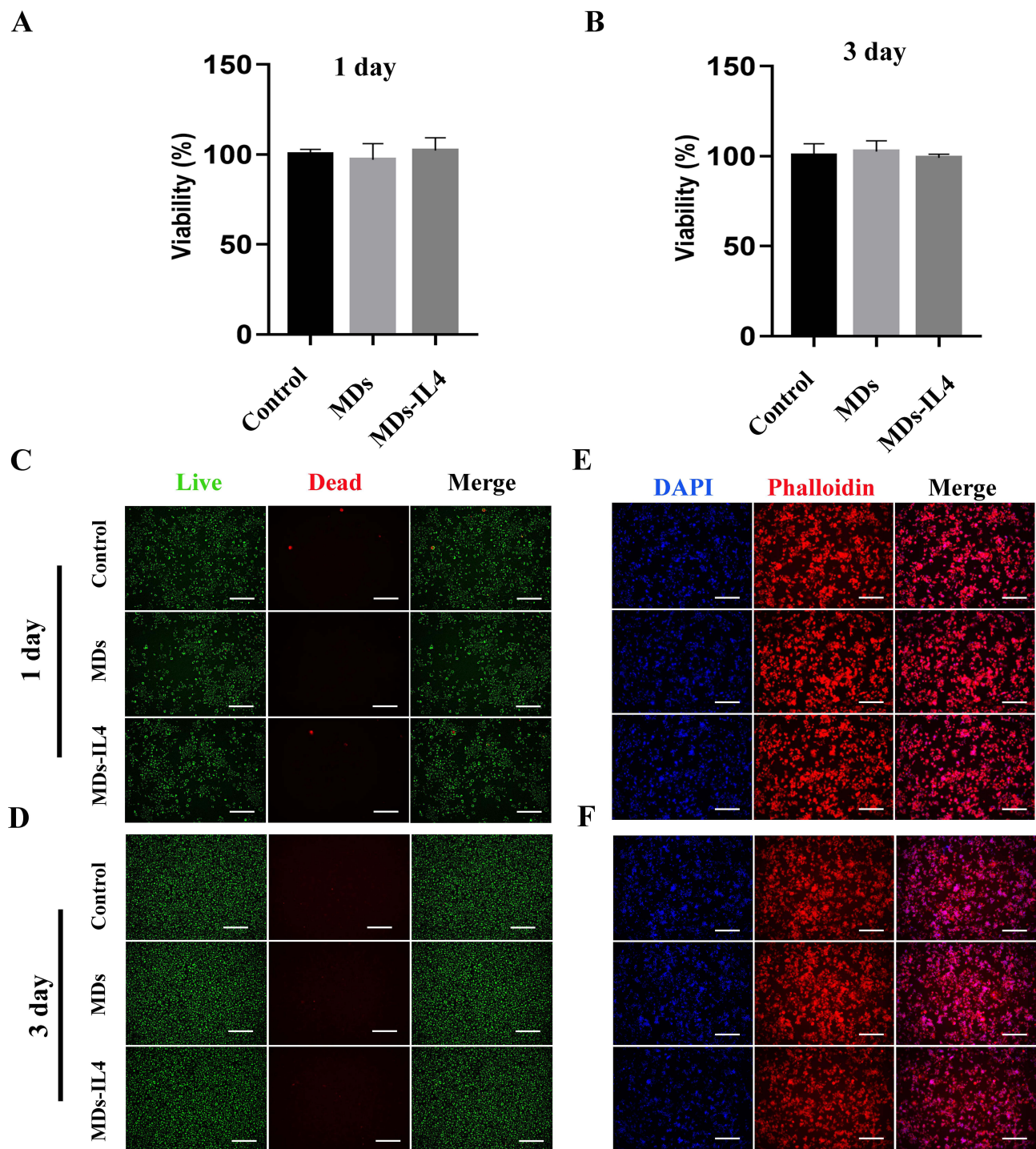
Figure 2 Cell viability of RAW264.7 macrophages treated with or without bioactive MDs. (**A** and **B**) Cell viability of RAW264.7 cells incubated with or without different formulations of MDs for 1 day and 3 days. Cell viability was determined by MTT assay. The data are presented as means ± SD (n = 3). (**C** and **D**) Representative CLSM images of live/dead staining of RAW264.7 cells incubated with or without different formulations of MDs. Viable cells were labeled as green color, while dead cells were marked with red color. Scale bar=250 μm. (**E** and **F**) Representative CLSM images of RAW264.7 macrophages treated with or without different formulations of MDs. Actin filaments were labeled using phalloidin (red), and the cell nuclei were stained with DAPI (blue). Scale bar = 250 μm.

Immunoregulatory Role of Bioactive MDs-IL4

To test the immunoregulatory properties of the bioactive MDs-IL4, we analyzed the inflammatory macrophage response following MDs and MDs-IL4 treatment. Macrophages were classically polarized into inflammatory phenotypes by LPS stimulation in vitro.[21] In this study, we observed that inflammatory macrophages treated with MDs-IL4 displayed markedly
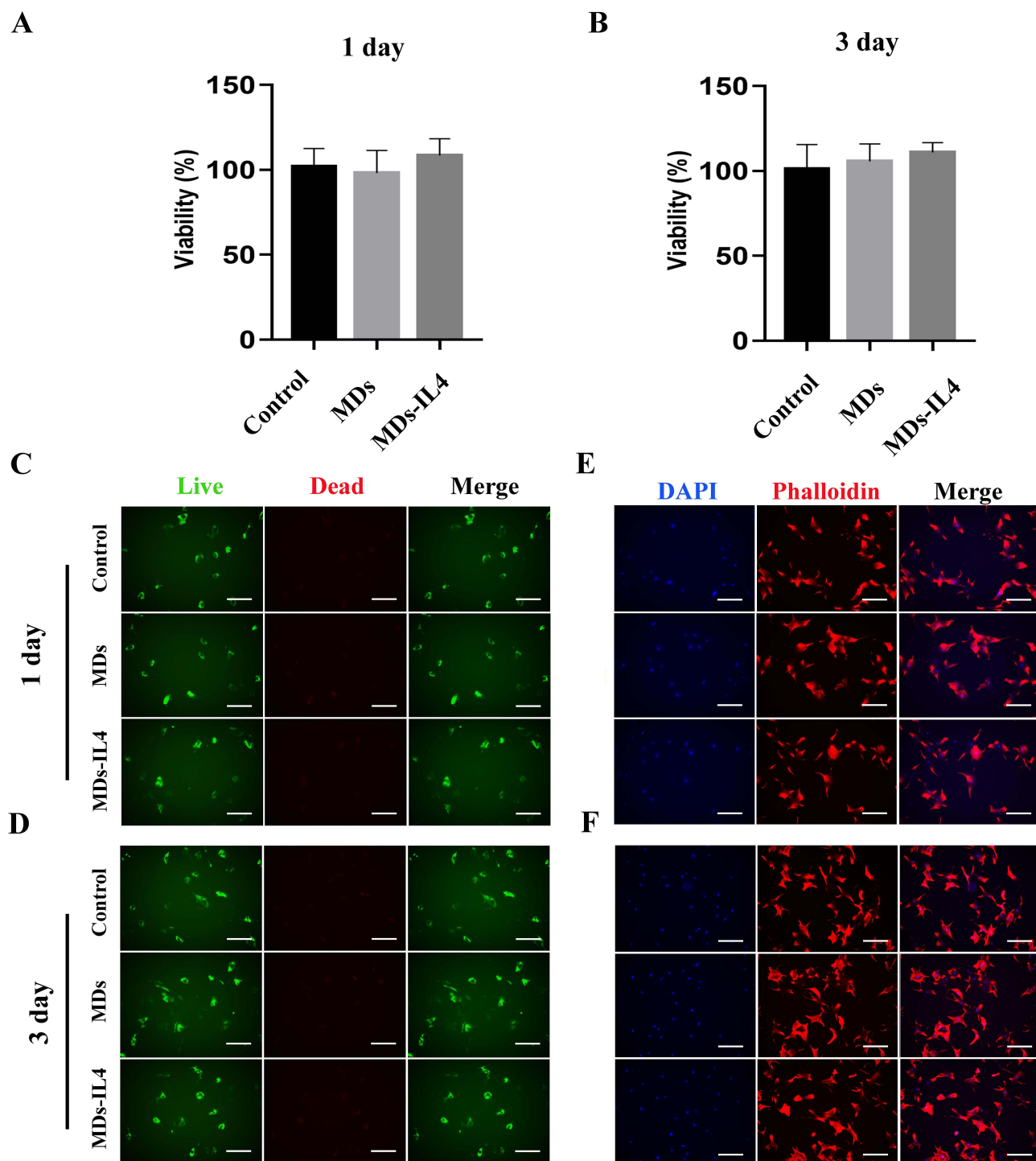
Figure 3 Cell viability of hBMSCs treated with or without bioactive MDs. (**A** and **B**) The effect of bioactive MDs on hBMSCs viability. hBMSCs were incubated with without different formulations of MDs for 1 day and 3 days. Cell viability was determined by MTT assay. The data are presented as means ± SD (n = 3). (**C** and **D**) CLSM images of live/dead staining of hBMSCs incubated with or without different formulations of MDs. Normal cells (green color) and dead cells (red color) are shown. Scale bar=250 μm. (**E** and **F**) Representative CLSM images of hBMSCs treated with or without different formulations of MDs. Actin filaments were labeled using phalloidin (red), and the cell nuclei were stained with DAPI (blue). Scale bar = 250 μm.

elongated cell morphologies compared to non-treated and MDs treated groups (Figure 4A), similar to the reports by other groups.[22,23]

Next, we used qPCR to determine the relative gene expression of proinflammatory markers in different groups. M1 macrophages are characterized by higher proinflammatory gene expression.[24] qPCR analysis revealed a significant
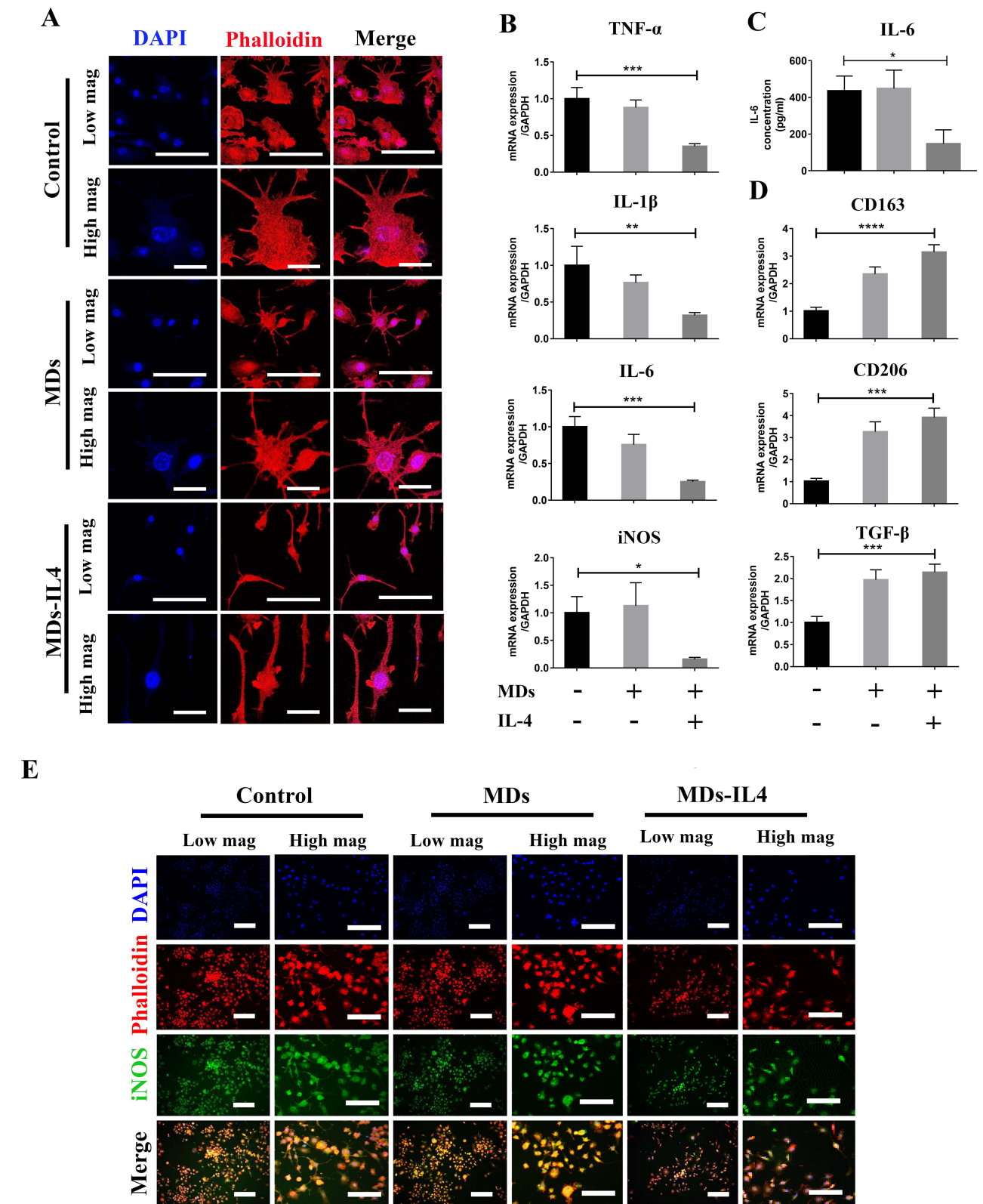
Figure 4 Immunoregulatory role of bioactive MDs-IL4 on inflammatory macrophages. (**A**) Representative CLSM images of RAW264.7 cells treated with or without different formulations of MDs. Inflammatory macrophages were induced via stimulation with 1000 ng/mL LPS. Actin filaments were labeled using phalloidin (red), and the cell nuclei were stained with DAPI (blue). Scale bar = 100 μm (low magnification). Scale bar = 20 μm (high magnification). (**B**) Relative mRNA expression of inflammation-related genes. Inflammatory macrophages were induced by LPS stimulation, followed by incubating with different formulations of MDs. GAPDH was used as housekeeping genes. All the results were expressed as mean ± SD (n = 3). Significant difference: *$p < 0.05$, **$p < 0.01$, ***$p < 0.001$. (**C**) IL-6 expression in the supernatant as measured by ELISA assay. All the results were expressed as mean ± SD (n = 3). * indicates statistically significant difference ($p < 0.05$). (**D**) Relative mRNA expression of anti-inflammatory-related genes. Significant difference: ***$p < 0.001$, ****$p < 0.0001$. (**E**) Representative CLSM images of RAW264.7 cells immunostained with iNOS (green), actin filament (red), and nuclei (blue) after treating with different formulation of MDs. Scale bar = 250 μm (low magnification). Scale bar = 100 μm (high magnification).

reduction of TNF-α, IL-1β, IL-6, and iNOS expression in M1 macrophages after treatment with bioactive MDs-IL4 (Figure 4B). The protein expression of pro-inflammatory IL-6 was further validated via ELISA. As indicated in Figure 4C, the result indicated that the amount of IL-6 in cell culture supernatant decreased significantly following bioactive MDs-IL4 treatment compared to control and MDs groups. In addition, classical M2 macrophage phenotypic markers for the identification of M2 macrophages, including CD206, CD163, and TGF-β, greatly increased following bioactive MDs-IL4 treatment (Figure 4D). These results indicated that MDs-IL4 offer unique immunoregulatory properties.

To further determine whether bioactive MDs-IL4 inhibits iNOS expression, the amount of iNOS in macrophages was examined by fluorescence staining analysis. As indicated in Figure 4E, the result indicated that the amount of iNOS intensity decreased significantly compared to control and MDs groups. In the control group, macrophages showed strong iNOS immunolabeling. However, macrophages with weaker iNOS fluorescent staining were observed in bioactive MDs-IL4 group, suggesting that iNOS expression was downregulated following MDs-IL4 treatment in macrophages.

Osteogenic Differentiation of hBMSCs

The osteogenic differentiation was first assessed by qPCR in hBMSCs cultured with CM derived from macrophages. Following treatment with MDs-IL4-CM, the expression of osteogenic-related markers (OSX, BSP, BMP-2, and ALP) significantly upregulated when compared to the control-CM and MDs-CM groups (Figure 5A).

To examine the role of MDs-IL4-CM on hBMSCs osteogenic differentiation, ALP expression was examined using immunofluorescence staining. On day 14, cells treated with MDs-IL4-CM displayed significantly higher ALP expression as evidenced by the immunofluorescence staining than that in the other two groups (Figure 5B).

To further evaluate the effect of MDs-IL4-CM on the osteogenic differentiation of hBMSCs, we evaluated the expression of ALP via ALP staining. The ALP staining result is presented in Figure 5C. The results indicated that cells treated with MDs-IL4-CM displayed significantly increased ALP levels compared to the control and MDs-CM treated groups.

Alizarin red S staining was further used to assess mineral deposits. As shown in Figure 5D, MDs-IL4-CM group demonstrated more alizarin red S staining compared to the control and MDs-CM treated groups. The alizarin red S quantification study further indicated that hBMSCs cultured in the presence of MDs-IL4-CM presented a significantly higher mineral deposition than the control and MDs-CM groups (Figure 5E).

In vivo Biocompatibility of the Bioactive MDs

To investigate the biocompatibility of bioactive MDs in vivo, we used H&E staining for the histopathological examination. As shown in Figure 6, no abnormal changes, necrosis, edema, inflammatory lesions or tissue damage, hemorrhage or other abnormalities were observed in the spleen, kidney, and lung after injection of bioactive MDs-IL4. Collectively, the H&E staining results indicated that there was good biocompatibility following bioactive MDs-IL4 injection.

Discussion

Current approaches for the treatment of fracture, and/or post-traumatic complications resulting from large bone defects remain unsatisfactory. M2 phenotypic macrophages play a key role in the repairing of the damaged tissues.[25] As one of the most important anti-inflammatory cytokines, IL-4 can polarize pro-inflammatory macrophages towards a tissue regenerative phenotype.[14] As one of the most commonly used non-invasive methods in the disease diagnosis and therapy, ultrasound and ultrasound-based drug delivery systems showed many advantages, including increased delivery efficiency, deep penetration nature, and controlled release of drugs.[15,26] Therefore, the purpose of this study was to investigate the possibility of fabricating ultrasound-responsive bioactive MDs with the incorporation of immunomodulatory cytokine, which could be used as a valuable therapeutic strategy to promote osteogenesis and tissue regeneration.

In recent years, it is now well acknowledged that skeletal and immune system are closely interacted with each other, where many cell types and molecular mediators are shared between these two systems.[27] It has been demonstrated that modulation of early osteoimmune environment will have significant impact for fracture healing.[20,21] In general, bone healing involves four specific biological phases: 1) initial inflammation phase, 2) soft callus phase, 3) hard callus
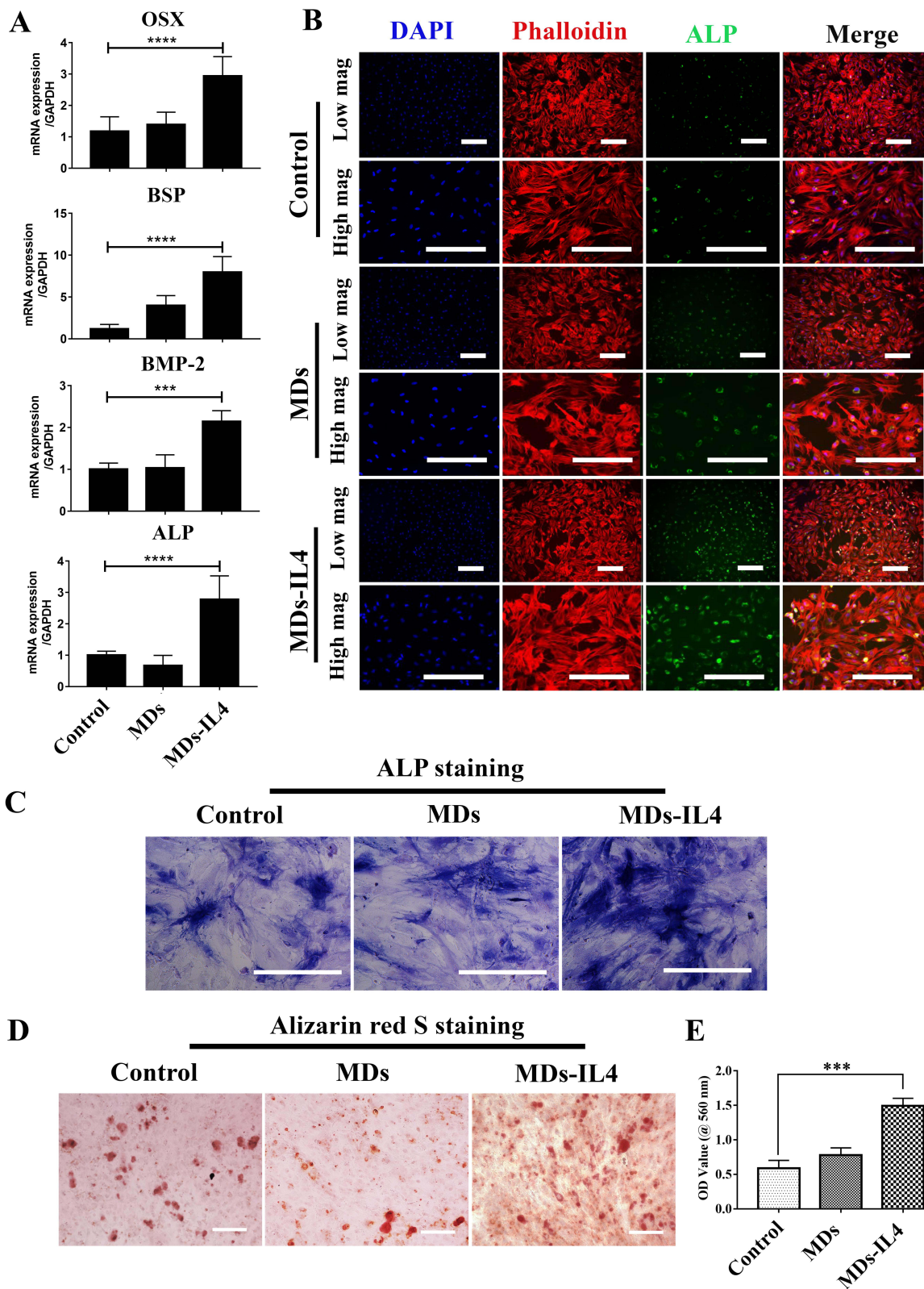
Figure 5 Osteogenic differentiation capacity of hBMSCs stimulated with macrophage-derived conditioned medium (CM). (**A**) Gene expression of osteogenic-related genes by qPCR after incubating with CM derived from macrophages. Significant difference ***$p < 0.001$, ****$p < 0.0001$. (**B**) Representative immunofluorescence staining images for osteogenic marker (ALP) in hBMSCs cultured with CM from macrophages. Scale bar=250 μm (low magnification), Scale bar=100 μm (high magnification). (**C**) ALP staining images of hBMSCs cultured with different scaffolds at days 14. Scale bar=100 μm. (**D**) Alizarin red S staining for calcium nodules formation at 21 days. Scale bar=250 μm. (**E**) Quantitative analysis of Alizarin red S staining in hBMSCs via CPC extraction method. 10% CPC in 10 mM phosphate buffer was used for alizarin red stain quantification. Significant difference: ***$p < 0.001$.
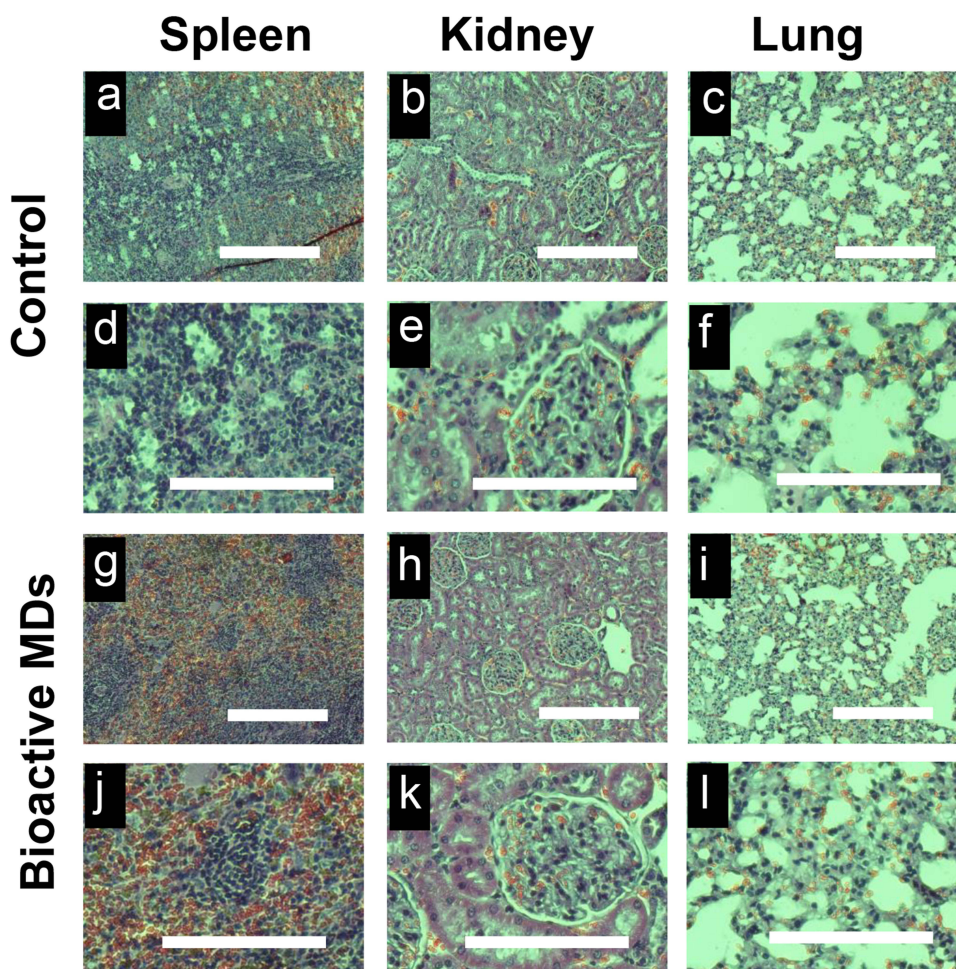
Figure 6 Biocompatibility of the bioactive MDs in vivo. Representative H&E staining images of the major rat organs (spleen, kidney, and lung) in control and bioactive MDs-IL4 treatment groups. No in vivo toxicity was observed. The image (**d–f** and **j–l**, scale bar = 200 µm) denotes the high magnification image from panels (**a–c** and **g–l**, scale bar = 200 µm).

formation, and 4) bone remodeling phase. The initial inflammatory phase is characterized by the formation of fracture hematoma, activation of the innate immune system, recruitment of immune and mesenchymal stem cells, and release of various cytokine and growth factor, etc.[24] Among all the immune cells, macrophages reside during all stages of bone regeneration, thus having a major impact on the long-term outcome of bone regeneration. For instance, Schlundt et al demonstrated a complete macrophage depletion via clodronate liposome injection resulted in delayed fracture healing.[28] In addition, Raggatt et al[29] depleted macrophages using Fas-induced apoptosis method in mice and investigated the impact of macrophage depletion on femoral fracture healing. Their results showed complete abolishment of callus formation when macrophages were depleted at the time of surgery, indicating the importance of macrophages for the initiation of fracture repair. Therefore, macrophages represent one of the most important immune cell types that is essential for tissue regeneration.[30]

In response to different external stimuli, macrophages can polarize into two different subtypes: pro-inflammatory M1 phenotype or anti-inflammatory alternative phenotype.[31] Pro-inflammatory M1 phenotypes produce high levels of pro-inflammatory cytokines (ie, TNF-α, IL-1β, and IL-6, etc) and reactive oxygen and nitrogen species, while anti-inflammatory alternative phenotypes are characterized by elevated expression of anti-inflammatory cytokines (ie, IL-4, IL-10, and IL-13, etc).[32] It is generally believed that M1 macrophages are the predominant subtypes at the early phase of bone regeneration, which play an important role in recruiting MSCs.[33] M2 macrophages increased at the later stage and function as pro-wound healing subtypes to stimulate tissue regeneration.[34] One of the most important key elements in
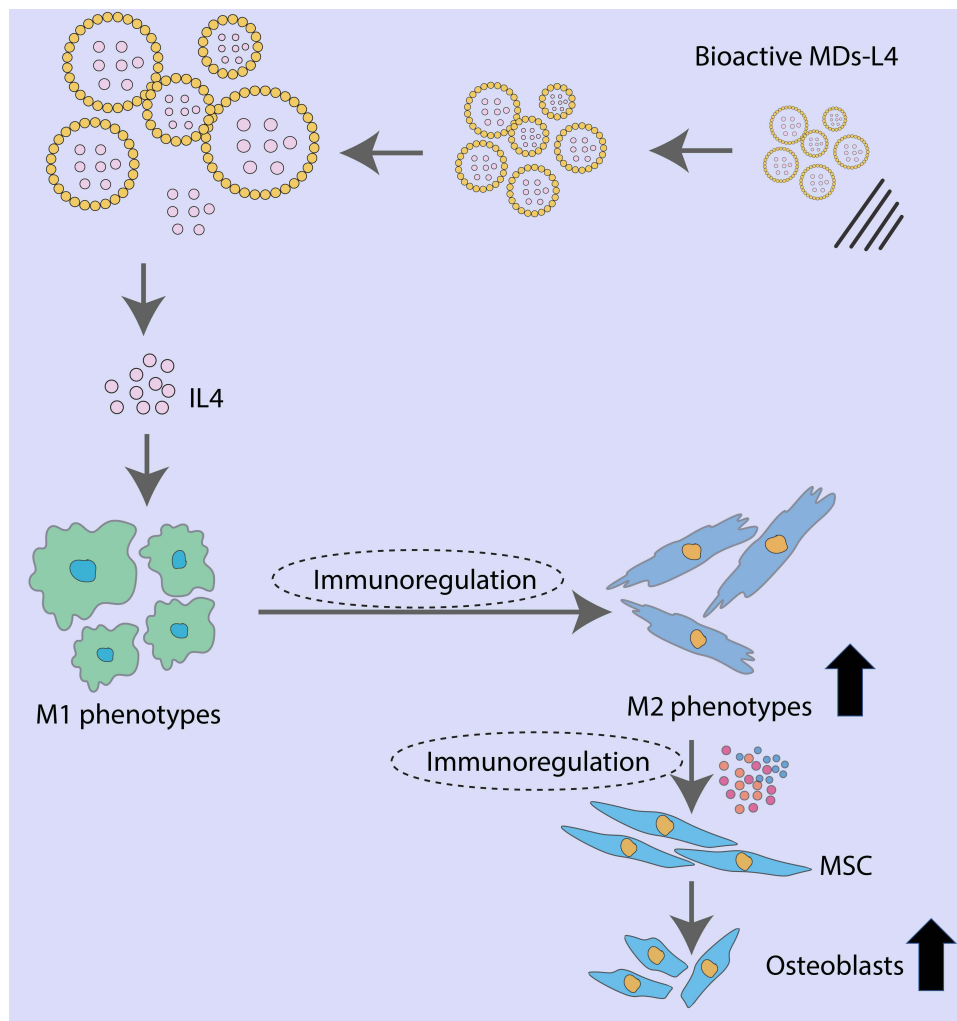
Figure 7 Schematic diagram showing the immunoregulatory role of MD-IL4. In this study, we fabricated a novel ultrasound-responsive bioactive MDs-IL4 to regulate macrophages polarization and potentiate the osteogenic differentiation of hBMSCs. The bioactive MDs-IL4 showed good response following ultrasound stimulation. In addition, the bioactive MDs-IL4 exhibited excellent biocompatibility in vitro and in vivo. It also demonstrated pro-osteogenic effect on hBMSCs differentiation via potential immunoregulatory role. The black upwards pointing arrows indicate increased M2 macrophages and enhanced osteogenesis, respectively.

bone regeneration is the prompt switch of macrophage phenotypes from pro-inflammatory M1 macrophage to the anti-inflammatory M2 phenotype. Successful switch from initial pro-inflammatory M1 macrophage to the anti-inflammatory M2 phenotype is very important for bone regeneration.

Although M1 macrophages are important for the initiation of the regeneration process, compromised bone regeneration is often associated with chronic inflammation, overproduction of reactive oxygen species (ROS), and prolonged inflammatory stage.[35] ROS play a central role in regulating inflammatory signaling and the progression of chronic disorders.[36] Mitochondrial function is essential for cell health and survival.[37] Over-production of ROS causes mitochondrial dysfunction and compromised differentiation potential of BMSCs.[38] Therefore, various therapeutic methods (eg, antioxidant-mediated) or bioactive scaffolds via immunomodulating the M1 to M2 macrophage transition have been developed to enhance the in vitro osteogenesis of mesenchymal stem cells and bone regeneration in vivo.[39] IL-4 is an anti-inflammatory cytokine, acting as an important regulator for controlling the release of proinflammatory cytokines and reactive oxygen species.[40] IL-4 has long been used alone as a regulatory molecule or in combination with other bioactive additives for scaffold modification for osteochondral repair or other disease models. For example, Tan et al developed an IL-4 coated bioactive vascular graft, which has the potential for promoting M2 macrophage polarization and inhibiting vascular grafts neointimal hyperplasia formation.[41] Zhang

et al also synthesized IL-4 encapsulated bioactive calcium-enriched gellan gum hydrogel beads, which could promote in vitro osteogenesis and in vivo bone regeneration.[42] Furthermore, Wei et al recently developed plasma immersion ion implantation (PIII)-activated polycaprolactone (PCL) surfaces with IL4-immobilization and found its unique osteo-immunoregulatory role of IL-4/PIII surface with significant pro-osteogenic effects when compared to bio-inert PCL surface.[21] Therefore, fabrication of bioactive materials capable of enhancing M1 to M2 phenotype transition, decreasing prolonged M1 macrophages or inflammation, and promoting pro-healing M2 macrophage populations have gained an increasing attention in recent years.

In this study, we tend to investigate the immunoregulatory role of MDs-IL4 in inflammatory macrophages. Macrophage morphology was commonly used to interpret the polarization subtypes by measuring cell areas, elongation ratio, etc.[43] Previous study demonstrated that M1 polarization displays pancake-like morphology, while M2 polarization causes cellular elongation.[22] Consistent with previous studies, our results here demonstrated M2 phenotypic polarization following bioactive MDs-IL4 treatment, as evidenced by elongated morphology and M2 phenotypic marker gene expression. Furthermore, the immunoregulatory roles of MDs-IL4 were further validated by significant reduction of pro-inflammatory marker gene expression and M1 phenotypic marker. Therefore, these results indicated that our MDs-IL4 offer unique immunoregulatory potential in polarizing inflammatory macrophages toward anti-inflammatory phenotypes.

IL-4 mediated therapies have the potential for creating a pro-healing microenvironment via macrophage immunomodulation.[42] MSCs are multi-potent cells with self-renewal and multi-directional differentiation potential, which can be isolated from various tissues, including umbilical cord,[44] bone marrow,[45] and adipose tissue,[46] etc. To investigate the immune-osteogenic response of hBMSCs to bioactive MDs-IL4 via macrophage and hBMSCs interaction, the osteogenesis of hBMSCs was further evaluated in vitro via osteogenic-related marker gene expression, ALP expression, and alizarin red S staining. Osterix (Osx) is a zinc finger-containing transcription factor, which plays an important role in osteoblast differentiation and bone mineralization.[47] Bone sialoprotein (BSP) is a glycosylated protein that is highly expressed by osteoblasts and during primary bone formation as depletion of BSP in mice showed reduced relatively low bone formation activity compared to normal control.[48,49] Bone morphogenetic protein 2 (BMP-2) belong to TGF-β superfamily, is known as a potent osteoinductive cytokine that regulates osteoblast differentiation and bone formation.[50] Alkaline phosphatase (ALP) is widely used as an early a biochemical marker of osteogenic differentiation.[51] Increased ALP expression by hBMSCs is important for bone formation and mineralization.[52] Our results further validated pro-osteogenic effect of MDs-IL4 via modulating macrophage polarization, as evidenced by higher levels of osteogenic-related markers and mineral deposition expression.

Conclusion

In the current study, we fabricated bioactive MDs with encapsulation of M2 macrophage inducer and investigated its role in regulating inflammatory macrophage response and osteogenic differentiation in hBMSCs (Figure 7). The bioactive MDs-IL4 showed good biocompatibility with no significant cellular toxicity in vitro and in vivo. It also demonstrated strong immunomodulatory effects on inflammatory macrophages and pro-osteogenic effect on the osteogenic differentiation, indicating that the bioactive MDs-IL4 could be used as a novel delivery system for other bioactive molecules, and therefore serve as therapeutic biomaterials for tissue or bone regeneration. However, there are many limitations to this study that need to be addressed in the future. For instance, as a proof of concept, we did not test the immunoregulatory and pro-healing properties of MDs-IL4 in bone defect model. Therefore, further research is warranted to evaluate its biological activity using in vivo studies. In addition, there is a need for further studies for the direct interaction between hBMSCs and MDs-IL4, especially its impact on hBMSCs immunoregulatory properties. In conclusion, this study may represent a pilot test to generate novel MDs-based delivery system for other immunoregulatory molecules for regulating bone tissue regeneration.

Data Sharing Statement

Please contact corresponding author for data requests.

Ethics Approval and Consent to Participate

Author Contributions

Funding

Disclosure

The authors declare that they have no competing interests.

References

1. G.B.D.F. Collaborators. Global, regional, and national burden of bone fractures in 204 countries and territories, 1990–2019: a systematic analysis from the Global Burden of Disease Study 2019. *Lancet Healthy Longev*. 2021;2(9):e580–e592. doi:10.1016/S2666-7568(21)00172-0
2. Pisani P, Renna MD, Conversano F, et al. Major osteoporotic fragility fractures: risk factor updates and societal impact. *World J Orthop*. 2016;7 (3):171–181. doi:10.5312/wjo.v7.i3.171
3. Augat P, von Ruden C. Evolution of fracture treatment with bone plates. *Injury*. 2018;49(Suppl 1):S2–S7. doi:10.1016/S0020-1383(18)30294-8
4. Jain A, Kumar S, Aggarwal AN, Jajodia N. Augmentation of bone healing in delayed and atrophic nonunion of fractures of long bones by partially decalcified bone allograft (decal bone). *Indian J Orthop*. 2015;49(6):637–642. doi:10.4103/0019-5413.168764
5. Sen MK, Miclau T. Autologous iliac crest bone graft: should it still be the gold standard for treating nonunions? *Injury*. 2007;38(Suppl 1):S75–S80. doi:10.1016/j.injury.2007.02.012
6. Khezri K, Maleki Dizaj S, Rahbar Saadat Y, et al. Osteogenic differentiation of mesenchymal stem cells via curcumin-containing nanoscaffolds. *Stem Cells Int*. 2021;(2021):1520052. doi:10.1155/2021/1520052
7. Li S, Feng S, Ding L, et al. Nanomedicine engulfed by macrophages for targeted tumor therapy. *Int J Nanomedicine*. 2016;11:4107–4124. doi:10.2147/IJN.S110146
8. Joorabloo A, Liu T. Recent advances in nanomedicines for regulation of macrophages in wound healing. *J Nanobiotechnology*. 2022;20(1):407. doi:10.1186/s12951-022-01616-1
9. Munoz J, Akhavan NS, Mullins AP, Arjmandi BH. Macrophage polarization and osteoporosis: a review. *Nutrients*. 2020;12(10):2999. doi:10.3390/nu12102999
10. Brown BN, Sicari BM, Badylak SF. Rethinking regenerative medicine: a macrophage-centered approach. *Front Immunol*. 2014;5:510. doi:10.3389/fimmu.2014.00510
11. Herold S, Hoegner K, Vadasz I, et al. Inhaled granulocyte/macrophage colony-stimulating factor as treatment of pneumonia-associated acute respiratory distress syndrome. *Am J Respir Crit Care Med*. 2014;189(5):609–611. doi:10.1164/rccm.201311-2041LE
12. Bykerk VP. The efficacy and safety of targeting GM-CSF in arthritis. *Lancet Rheumatol*. 2020;2(11):e648–e650. doi:10.1016/S2665-9913(20)30352-0
13. Gong L, Li J, Zhang J, et al. An interleukin-4-loaded bi-layer 3D printed scaffold promotes osteochondral regeneration. *Acta Biomater*. 2020;117:246–260. doi:10.1016/j.actbio.2020.09.039
14. Ueno M, Lo CW, Barati D, et al. Interleukin-4 overexpressing mesenchymal stem cells within gelatin-based microribbon hydrogels enhance bone healing in a murine long bone critical-size defect model. *J Biomed Mater Res A*. 2020;108(11):2240–2250. doi:10.1002/jbm.a.36982
15. Cai X, Jiang Y, Lin M, et al. Ultrasound-responsive materials for drug/gene delivery. *Front Pharmacol*. 2019;10:1650.
16. Su C, Ren X, Nie F, et al. Current advances in ultrasound-combined nanobubbles for cancer-targeted therapy: a review of the current status and future perspectives. *RSC Adv*. 2021;11(21):12915–12928. doi:10.1039/D0RA08727K
17. Lentacker I, Geers B, Demeester J, De Smedt SC, Sanders NN. Design and evaluation of doxorubicin-containing microbubbles for ultrasound-triggered doxorubicin delivery: cytotoxicity and mechanisms involved. *Mol Ther*. 2010;18(1):101–108. doi:10.1038/mt.2009.160
18. Shar A, Aboutalebianaraki N, Misiti K, Sip YYL, Zhai L, Razavi M. A novel ultrasound-mediated nanodroplet-based gene delivery system for osteoporosis treatment. *Nanomedicine*. 2022;41:102530. doi:10.1016/j.nano.2022.102530

19. Lee WT, Yoon J, Kim SS, et al. Combined antitumor therapy using in situ injectable hydrogels formulated with albumin nanoparticles containing indocyanine green, chlorin e6, and perfluorocarbon in hypoxic tumors. *Pharmaceutics*. 2022;14(1):148.

20. Wei F, Zhou Y, Wang J, Liu C, Xiao Y. The immunomodulatory role of BMP-2 on macrophages to accelerate osteogenesis. *Tissue Eng Part A*. 2018;24(7–8):584–594. doi:10.1089/ten.tea.2017.0232

21. Wei F, Mu Y, Tan RP, et al. Osteo-immunomodulatory role of interleukin-4-immobilized plasma immersion ion implantation membranes for bone regeneration. *ACS Appl Mater Interfaces*. 2023;15(2):2590–2601. doi:10.1021/acsami.2c17005

22. McWhorter FY, Wang T, Nguyen P, Chung T, Liu WF. Modulation of macrophage phenotype by cell shape. *Proc Natl Acad Sci U S A*. 2013;110 (43):17253–17258. doi:10.1073/pnas.1308887110

23. Fraser AR, Pass C, Burgoyne P, et al. Campbell, Development, functional characterization and validation of methodology for GMP-compliant manufacture of phagocytic macrophages: a novel cellular therapeutic for liver cirrhosis. *Cytotherapy*. 2017;19(9):1113–1124. doi:10.1016/j. jcyt.2017.05.009

24. Oishi Y, Manabe I. Macrophages in inflammation, repair and regeneration. *Int Immunol*. 2018;30(11):511–528. doi:10.1093/intimm/dxy054

25. Sapudom J, Karaman S, Mohamed WKE, Garcia-Sabate A, Quartey BC, Teo JCM. 3D in vitro M2 macrophage model to mimic modulation of tissue repair. *NPJ Regen Med*. 2021;6(1):83. doi:10.1038/s41536-021-00193-5

26. Delaney LJ, Isguven S, Eisenbrey JR, Hickok NJ, Forsberg F. Making waves: how ultrasound-targeted drug delivery is changing pharmaceutical approaches. *Mater Adv*. 2022;3(7):3023–3040. doi:10.1039/D1MA01197A

27. Mori G, D'Amelio P, Faccio R, Brunetti G. The Interplay between the bone and the immune system. *Clin Dev Immunol*. 2013;(2013):720504. doi:10.1155/2013/720504

28. Schlundt C, El Khassawna T, Serra A, et al. Macrophages in bone fracture healing: their essential role in endochondral ossification. *Bone*. 2018;106:78–89. doi:10.1016/j.bone.2015.10.019

29. Raggatt LJ, Wullschleger ME, Alexander KA, et al. Fracture healing via periosteal callus formation requires macrophages for both initiation and progression of early endochondral ossification. *Am J Pathol*. 2014;184(12):3192–3204. doi:10.1016/j.ajpath.2014.08.017

30. Wynn TA, Vannella KM. Macrophages in tissue repair, regeneration, and fibrosis. *Immunity*. 2016;44(3):450–462. doi:10.1016/j. immuni.2016.02.015

31. Yao Y, Xu XH, Jin L. Macrophage polarization in physiological and pathological pregnancy. *Front Immunol*. 2019;10:792. doi:10.3389/ fimmu.2019.00792

32. Saqib U, Sarkar S, Suk K, Mohammad O, Baig MS, Savai R. Phytochemicals as modulators of M1-M2 macrophages in inflammation. *Oncotarget*. 2018;9(25):17937–17950. doi:10.18632/oncotarget.24788

33. Pajarinen J, Lin T, Gibon E, et al. Mesenchymal stem cell-macrophage crosstalk and bone healing. *Biomaterials*. 2019;196:80–89. doi:10.1016/j. biomaterials.2017.12.025

34. Niu Y, Wang Z, Shi Y, Dong L, Wang C. Modulating macrophage activities to promote endogenous bone regeneration: biological mechanisms and engineering approaches. *Bioact Mater*. 2021;6(1):244–261. doi:10.1016/j.bioactmat.2020.08.012

35. Maruyama M, Rhee C, Utsunomiya T, et al. Modulation of the inflammatory response and bone healing. *Front Endocrinol*. 2020;11:386. doi:10.3389/fendo.2020.00386

36. Mittal M, Siddiqui MR, Tran K, Reddy SP, Malik AB. Reactive oxygen species in inflammation and tissue injury. *Antioxid Redox Signal*. 2014;20 (7):1126–1167. doi:10.1089/ars.2012.5149

37. Chodari L, Dilsiz Aytemir M, Vahedi P, et al. Targeting mitochondrial biogenesis with polyphenol compounds. *Oxid Med Cell Longev*. 2021;2021:4946711. doi:10.1155/2021/4946711

38. Yan W, Diao S, Fan Z. The role and mechanism of mitochondrial functions and energy metabolism in the function regulation of the mesenchymal stem cells. *Stem Cell Res Ther*. 2021;12(1):140. doi:10.1186/s13287-021-02194-z

39. Xiang G, Liu K, Wang T, et al. In situ regulation of macrophage polarization to enhance osseointegration under diabetic conditions using injectable silk/sitagliptin gel scaffolds. *Adv Sci*. 2021;8(3):2002328. doi:10.1002/advs.202002328

40. Celik MO, Labuz D, Keye J, Glauben R, Machelska H. IL-4 induces M2 macrophages to produce sustained analgesia via opioids. *JCI Insight*. 2020;5(4). doi:10.1172/jci.insight.133093

41. Tan RP, Chan AHP, Wei S, et al. Bioactive materials facilitating targeted local modulation of inflammation. *JACC Basic Transl Sci*. 2019;4 (1):56–71. doi:10.1016/j.jacbts.2018.10.004

42. Zhang J, Shi H, Zhang N, Hu L, Jing W, Pan J. Interleukin-4-loaded hydrogel scaffold regulates macrophages polarization to promote bone mesenchymal stem cells osteogenic differentiation via TGF-beta1/Smad pathway for repair of bone defect. *Cell Prolif*. 2020;53(10):e12907. doi:10.1111/cpr.12907

43. Lee HS, Stachelek SJ, Tomczyk N, Finley MJ, Composto RJ, Eckmann DM. Correlating macrophage morphology and cytokine production resulting from biomaterial contact. *J Biomed Mater Res A*. 2013;101(1):203–212. doi:10.1002/jbm.a.34309

44. Nguyen LT, Tran NT, Than UTT, et al. Optimization of human umbilical cord blood-derived mesenchymal stem cell isolation and culture methods in serum- and xeno-free conditions. *Stem Cell Res Ther*. 2022;13(1):15. doi:10.1186/s13287-021-02694-y

45. Baghaei K, Hashemi SM, Tokhanbigli S, et al. Isolation, differentiation, and characterization of mesenchymal stem cells from human bone marrow. *Gastroenterol Hepatol Bed Bench*. 2017;10(3):208–213.

46. Vahedi P, Moghaddamshahabi R, Webster TJ, et al. The use of infrapatellar fat pad-derived mesenchymal stem cells in articular cartilage regeneration: a review. *Int J Mol Sci*. 2021;22(17):9215. doi:10.3390/ijms22179215

47. Liu Q, Li M, Wang S, Xiao Z, Xiong Y, Wang G. Recent advances of osterix transcription factor in osteoblast differentiation and bone formation. *Front Cell Dev Biol*. 2020;8:601224. doi:10.3389/fcell.2020.601224

48. Malaval L, Wade-Gueye NM, Boudiffa M, et al. Bone sialoprotein plays a functional role in bone formation and osteoclastogenesis. *J Exp Med*. 2008;205(5):1145–1153. doi:10.1084/jem.20071294

49. Bouet G, Bouleftour W, Juignet L, et al. The impairment of osteogenesis in bone sialoprotein (BSP) knockout calvaria cell cultures is cell density dependent. *PLoS One*. 2015;10(2):e0117402. doi:10.1371/journal.pone.0117402

50. Lee SS, Huang BJ, Kaltz SR, et al. Bone regeneration with low dose BMP-2 amplified by biomimetic supramolecular nanofibers within collagen scaffolds. *Biomaterials*. 2013;34(2):452–459. doi:10.1016/j.biomaterials.2012.10.005

51. Li N, Zhou L, Xie WL, et al. Alkaline phosphatase enzyme-induced biomineralization of chitosan scaffolds with enhanced osteogenesis for bone tissue engineering. *Chem Eng J.* 2019;371:618–630. doi:10.1016/j.cej.2019.04.017

52. Cheng CH, Shie MY, Lai YH, Foo NP, Lee MJ, Yao CH. Fabrication of 3D printed poly(lactic acid)/polycaprolactone scaffolds using TGF-beta1 for promoting bone regeneration. *Polymers.* 2021;13(21):3731. doi:10.3390/polym13213731